Taylor & Francis
Taylor & Francis Group

Advanced Robotics iFirst (2012) 1–22

ADVANCED ROBOTICS
tandfonline.com/tadr

Full paper

Virtual Chassis for Snake Robots: Definition and Applications

David Rollinson*, Austin Buchan and Howie Choset

The Robotics Institute, Carnegie Mellon University, 5000 Forbes Avenue, Pittsburgh, PA 15203, USA

Received 9 March 2012; accepted 22 May 2012

Abstract

Intuitively representing the motion of a snake robot is difficult. This is in part because the internal shape changes that the robot uses to locomote involve the entire body and no single point on the robot intuitively represents the robot's pose at all times. To address this issue, we present a method of defining body coordinate frames that departs from the typical convention of rigidly fixing a frame to a link on the robot, and instead define a body frame that is based on the averaged position of all of the robot's links. This averaged frame serves as a *virtual chassis* that effectively isolates the internal motion of the robot's shape changes from the external motion, due to the robot's interaction with its surroundings. This separation of motion allows much simpler models—such as those derived for wheeled vehicles—to accurately approximate the motion of the robot as it moves through the world. We demonstrate the practical advantages of using the virtual chassis body frame by estimating the pitch and roll of a snake robot undergoing dynamic motion by fusing readings from its internal encoders, gyros, and accelerometers with an extended Kalman filter.

Keywords

snake robot, body frame, gaits, state estimation

1. Introduction

Snake robots are a class of hyper-redundant mechanisms [1] consisting of kinematically constrained links chained together in series, whose many degrees of freedom allow them to navigate a wide range environments. Our group has developed modular snake robots that rely solely on their internal shape changes to locomote through their environment [2]. To simplify control of the robot's many degrees of freedom, cyclic motions, known as *gaits*, are used to undulate the robot's joints according to parameterized periodic functions, such as sine

*To whom correspondence should be addressed. Email: drollins@cs.cmu.edu

 DOI: 10.1080/01691864.2012.728695

waves [3]. Our research group, as well as others [4], has developed and implemented gaits that can traverse a variety of terrains, including flat ground and pipes, as shown in Figure 1.

Despite the community's success in developing snake robot gaits, a significant, yet overlooked, challenge remains: how to represent a snake robot's motion. In particular, defining a body frame in which to intuitively describe the robot's motion in the world is difficult. To illustrate this problem, consider a simple two-wheeled differential drive robot with a body frame fixed to the center of the robot's chassis. Operating such a device is easy, because the notions of 'forward' or 'up' are clearly defined, and the robot's wheels propel it smoothly through the world. Put in more technical terms, the robot's definition of pose is independent from its internal shape changes (the turning of the wheels), and its controls, which are executed in the body frame, map intuitively into a world frame. With snake robots, an operator can still control the robot with some sense of its position and orientation by simply looking at the robot. However, the intuition for this frame lies solely with the operator, and is drawn from observing the robot as a whole rather than any individual link.

Figure 1. Examples of our snake robot executing the gaits discussed in this paper. From top left to bottom right: sidewinding, rolling, pipe crawling, and pole climbing.

Our goal is to formally define a body frame that embodies this intuition. In this paper, we show that using a body frame whose origin is the robot's center of mass and whose axes are aligned with the robot's principal moments of inertia is one where the intuitive notions of position and orientation prevail. We refer to this frame as a *virtual chassis* because, like the chassis of a car, it isolates a robot's internal shape changes from its external motions, allowing us to think of snake robots more like wheeled vehicles.

Even though the virtual chassis itself is just a choice of body frame, we can use it to aid in the planning and estimation of snake robots. For example, we can leverage the advantages of the virtual chassis to enable the accurate estimation of the robot's orientation using its internal gyros and accelerometers. Normally, this would be a difficult task, since we lack an accurate model for how the robot moves in the world in response to its internal shape changes. However, we show that by using the virtual chassis, rather than a fixed body frame, we can greatly simplify the apparent motion of the robot through the world. This allows a generic constant velocity model to be successfully used as the underlying model of the state estimator, even for very dynamic motions.

2. Prior Work

There is a significant amount prior work in the study of the motion of biological snakes [5,6] and snake robots [1,7–14], these being only a selection of the works available. More recent research on both biological snakes [15] and robotic snakes [16,17] has focused on a snake robot's interaction with its environment during locomotion. While such work is undoubtedly leading to fundamental scientific discovery, our work takes a different perspective in which we do not directly consider robot interaction with the world. Instead, our approach seeks ways to formally represent the macroscopic motion of the robot, allowing us to abstract away the details of ground contact and friction.

Using an averaged approximation of a system as a way of providing intuition to a system's analysis and control has been explored in other contexts. For planar swimming systems, Shapere and Wilczek [18] use the center of mass and principal axes to define body frames for irregularly shaped bodies. In the field of humanoid robotics, Kajita et al. [19] use the pseudo inverse of the inertia matrix to quickly generate whole body motions where the linear and angular momenta are controlled.

In many ways, our work is inspired by the work of Hatton and Choset [20], who demonstrate that a good choice of body frame can greatly simplify motion planning for planar systems. By exploiting a system's known dynamics, they are able optimize the coordinate frame to be one in which a locomoting system moves the least in response to changes in its shape. Using these minimum perturbation coordinates, they are able to identify effective gaits by representing the system dynamics as geometric functions over the system's shape space.

While we lack the specific constraints needed to define optimal coordinate frames in their manner, our work draws on their observation that their optimal body frame is often aligned with the intuitive notions of center of mass and mean orientation.

There is a wealth of prior work for state estimation in robotics systems. Methods for fusing redundant data in robotics systems are surveyed by Luo et al. [21]. There is also a long history of using the extended Kalman filter and other methods for orientation estimation [22–24].

3. Virtual Chassis

The first part of this paper presents a general procedure for calculating the virtual chassis body frame. We begin by presenting some background on the kinematic configuration of our snake robots and the gait equations that is used for control, and then detail the method of calculating the virtual chassis, given knowledge of the robot's shape. The overall procedure involves continually aligning the body frame with the robot's principle moments of inertia. Specifically, this is done by taking the singular value decomposition (SVD) of the positions of all of the robot's links with respect to the robot's center of mass at discrete time steps as the robot executes the gait.

3.1. Gaits and Robot Kinematics

Our snake robots consist of 16 (or more) links where single degree of freedom rotary joints are alternately oriented in the lateral and dorsal planes of the robot [25]. Because of this design, our gait equations consist of separate waves that propagate through the lateral and dorsal joints. These undulations typically follow parameterized sinusoidal backbone curvatures that are based on Hirose's serpenoid curve [7], and its 3D extensions [26]. We refer to these equations as the *compound serpenoid curve*,

$$\theta(i,t) = \begin{cases} \beta_{\text{lat}} + A_{\text{lat}} \sin(\xi_{\text{lat}}) & \text{lateral joints} \\ \beta_{\text{dor}} + A_{\text{dor}} \sin(\xi_{dor} + \delta) & \text{dorsal joints} \end{cases} \tag{1}$$

$$\begin{aligned} \xi_{\text{lat}} &= \Omega_{\text{lat}} i + \upsilon_{\text{lat}} t \\ \xi_{\text{dor}} &= \Omega_{\text{dor}} i + \upsilon_{\text{dor}} t. \end{aligned} \tag{2}$$

In (1) β, A and δ are respectively the angular offset, amplitude, and phase shift between the lateral and dorsal joint waves. In (2), the parameter Ω describes the spatial frequency of the waves with respect to link number, i. The temporal component υ determines the frequency of the actuator cycles with respect to time, t.

3.2. Calculating the Virtual Chassis Body Frame

Given an arbitrarily chosen body frame, such as one fixed to the head link (Figure 2), we can use standard kinematics to calculate the poses of all the links on the robot with respect to this frame [27]. We then find the translation and rotation from this initial frame to the frame aligned with the principle moments of inertia taken about the center of mass. We then transform the pose of each link of the robot from the initial frame to this new frame, thereby representing the robot's pose in the virtual chassis.

The first step is to find the geometric center of mass of the robot $\bar{x}$, $\bar{y}$, and $\bar{z}$ in the initial frame. We then construct a data matrix of the positions of the links $\mathbf{p_i}$, subtracting out the center of mass. This matrix, $\mathbf{P}$ will be of size $n \times 3$, where n is the number of links and each row i corresponds to the ith link in the robot,

$$Pi = [x_i - \bar{x} \quad y_i - \bar{y} \quad z_i - \bar{z}] \tag{3}$$

$$\mathbf{P} = \begin{bmatrix} \mathbf{p_1} \\ \vdots \\ \mathbf{p_n} \end{bmatrix}. \tag{4}$$

Now that the origin of the initial coordinate frame is at the center of mass, the next step is to find a rotation such that the principal axes of the body frame are aligned with the principal moments of inertia of the link positions around the center of mass. To find this rotation, we take the SVD of $\mathbf{P}$. SVD decomposes this matrix into 3 new matrices,

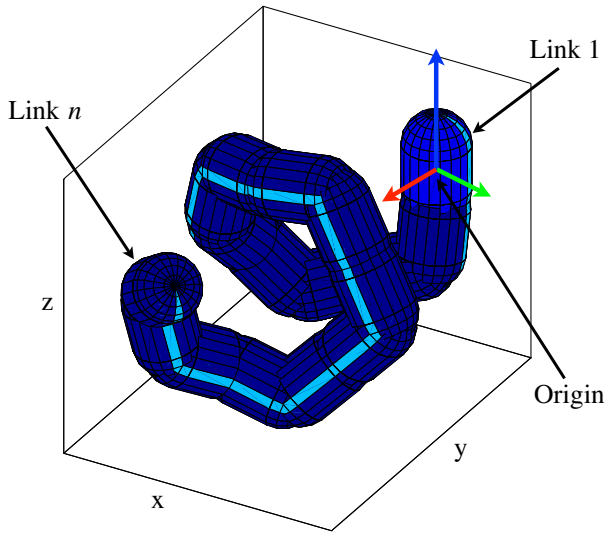

Figure 2. An example of an arbitrary initial body frame for the robot that is fixed to the head link.

$$\mathbf{USV}^T = \mathbf{P}. \tag{5}$$

In the decomposition, $\mathbf{U}$ and $\mathbf{V}$ are unitary matrices whose columns are respectively the left and right singular vectors of $\mathbf{P}$. The columns of $\mathbf{U}$ are eigenvectors of $\mathbf{PP}^T$, meaning that they form an orthonormal basis in $\mathbb{R}^n$. Likewise, the columns of $\mathbf{V}$ are eigenvectors of $\mathbf{P}^T\mathbf{P}$ and form an orthonormal basis in $\mathbb{R}^3$. This means that $\mathbf{V}$ serves as a rotation matrix that describes the orientation of the coordinate frame aligned with the principal moments of inertia, described in initial coordinate frame. The diagonal elements of $\mathbf{S}$ are the singular values of $\mathbf{P}$. They correspond to the square roots of the eigenvalues of $\mathbf{P}^T\mathbf{P}$ and describe the magnitudes of the principal moments of inertia. More detail on SVD can be found in [28,29].

A technical detail to note about SVD is that $\mathbf{V}$ is only unique up to a reflection about each singular vector [30]. To ensure right-handed coordinates, at each timestep $\mathbf{V}$ is modified such that the third singular vector is defined to be the cross product of the first and second singular vectors. To avoid sign flips in $\mathbf{V}$ across later timesteps, we respectively enforce positive dot products between the first and second singular vectors at the current timestep and those of the previous timestep.

Combining the rotation matrix $\mathbf{V}$ with the center of mass $\bar{\mathbf{p}}$, we have the homogeneous transform that describes the pose of the virtual chassis with respect to the initial body frame,

$$\mathbf{T} = \begin{bmatrix} \mathbf{V} & \bar{\mathbf{p}} \\ 0 & 1 \end{bmatrix}. \tag{6}$$

The last step is to transform the pose of each link in the robot to the virtual chassis body frame. If the pose of each link is described by a homogeneous transform, left multiplying each link's transform by $\mathbf{T}^{-1}$ now represents its pose in the virtual chassis body frame.

4. Implementation

Our lab has developed a variety of gaits for our snake robots, including sidewinding, rolling, pipe crawling, and pole climbing (Figure 1). For each of these gaits, we demonstrate calculating the virtual chassis via SVD as outlined in the previous section. Note that this general procedure can be applied to any body shape that has distinct principle components, including noncyclic motions and transitions between gaits. For gaits designed specifically to traverse pipes, we can further refine the virtual chassis to exploit the structure of the robot's shape, better aligning the body frame with centerline of the pipe.

4.1. Sidewinding

The sidewinding gait (Figure 3) is characterized by a series of lateral and dorsal undulations that form a rolling tread [31,32]. This motion corresponds to a phase offset of $\pi/4$ in the serpenoid equations (1). The overall shape of the robot in sidewinding can be described as a helix with an elliptical cross-section. This body shape has the property that the longest, middle, and shortest dimensions that are clearly defined and are orthogonal.

For sidewinding, the procedure for calculating the virtual chassis follows the general procedure from Section 3. At each new timestep, a new $\mathbf{P}$ is calculated from the robot's joint angles and a new body frame is defined. A comparison of sidewinding motion in an initial head-fixed body frame and the virtual chassis body frame is shown in Figure 4. Note that the motion of the robot in virtual chassis body frame captures the 'rolling tread' motion of the gait, compared to the side-to-side motion that is apparent in a fixed body frame.

4.2. Rolling

In the basic rolling gait, the robot forms a static backbone shape, consisting of an arc of constant curvature, and then rolls within that shape (Figure 5). This constant curvature corresponds to setting the spatial frequency Ω in (2) to 0, and setting the phase offset between the lateral and dorsal joint angles, δ from (1) to $\pi/2$ radians.

As the robot cycles through the gait over flat terrain, the arc remains level on the ground and the robot rolls either toward or away from the center of the arc. Like sidewinding, the shape of the robot in rolling has clearly defined longest, middle, and shortest dimensions to its shape.

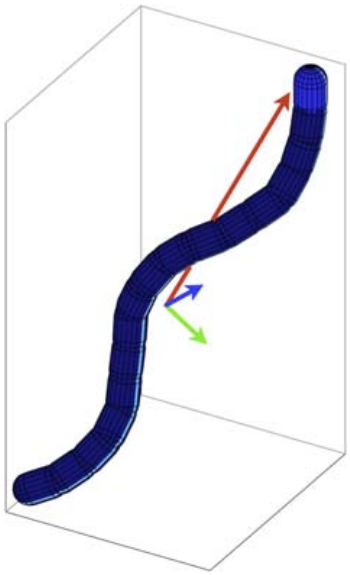

Figure 3. An example of the approximate axes of the virtual chassis for the sidewinding gait.

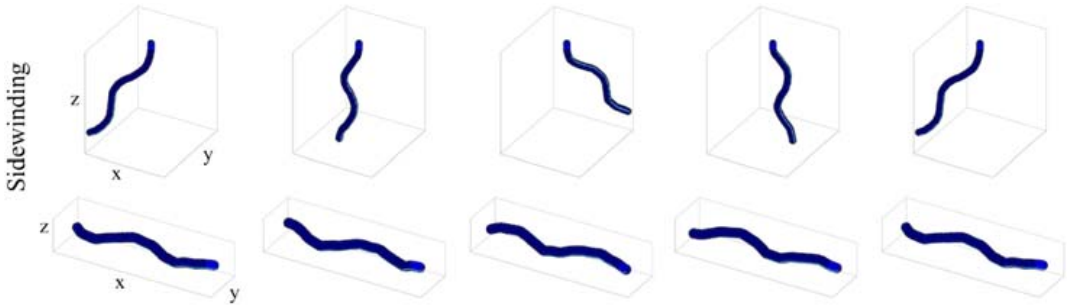

Figure 4. A montage of the robot in sidewinding, shown in five different positions spaced evenly throughout one complete gait cycle. The top row of images shows the pose of the robot in a body frame fixed to the head link. The bottom row shows the pose corresponding to the virtual chassis body fame at the same points in the gait cycle.

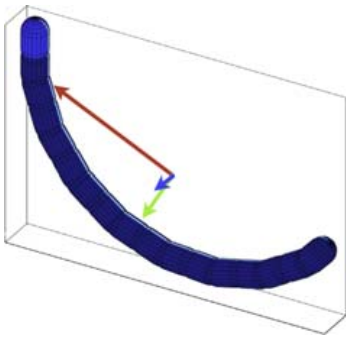

Figure 5. An example of the approximate axes of the virtual chassis for the rolling gait.

For this gait, we align the first, second, and third principal moments of inertia respectively with the x, y, and z axes of the body frame. The procedure for calculating the virtual chassis for rolling follows the general procedure. A comparison of the motions of the rolling gait in an initial head-fixed body frame and the virtual chassis body frame is shown in Figure 6. Note that the motion of the robot in virtual chassis body frame matches the gait's internal twisting motion, compared to the sweeping motion that is apparent in a fixed body frame.

4.3. Helix – Pipe Crawling

The helix gait is useful for traveling along cylindrical surfaces, like the pipes in Figure 1. Like the rolling gait, it is characterized by a static backbone shape in which the robot twists, again produced by a $\pi/2$ phase offset in the lateral and dorsal joint angles δ. However, in this case a nonzero spatial frequency Ω causes the base backbone shape of the gait to form a cylindrical helix, rather than a flat arc (Figure 7). Pipe crawling is a parameterization of helix in which Ω is chosen to create approximately 1.5 wave cycles over the length of the robot.

The shape of the robot in pipe crawling has a clearly defined longest direction, corresponding to the first principal moment of inertia. However, in this

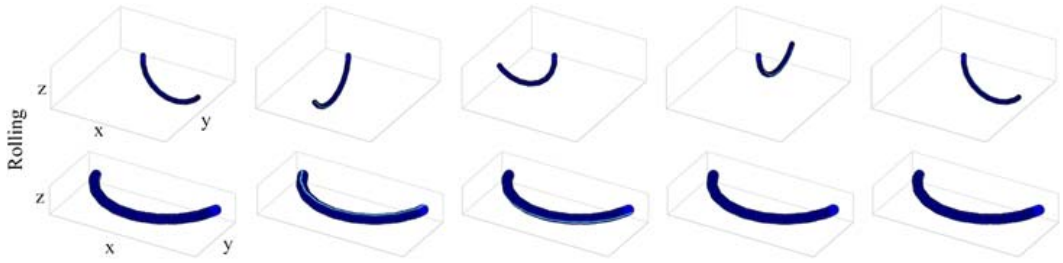

Figure 6. A montage of the robot in rolling, comparing the motions in a body frame fixed to the head link (top row) and the virtual chassis body frame (bottom row).

gait, the second and third moments of inertia are less distinct. This makes intuitive sense, since for a true cylinder the second and third moments are exactly equal, due to symmetry about the cylinder's axis. Since the robot consists of a finite number of links, significant asymmetry is present, and SVD will still find an unambiguous solution for the virtual chassis.

As with the gaits discussed so far, the resulting body frame using the general procedure isolates the robot's internal and external motions. However, since this gait is used specifically for locomoting on the inside of pipes (bottom left of Figure 1), we can exploit the known constraints of the environment and define a more useful body frame that is better aligned with the true centerline of the robot's helical shape (as well as centerline of the pipe).

To find the true centerline of the robot, we take the initial solution from SVD and use it as the starting point of optimization using the Nelder-Mead simplex search [33]. Intuitively, we would like to minimize the difference of the distances

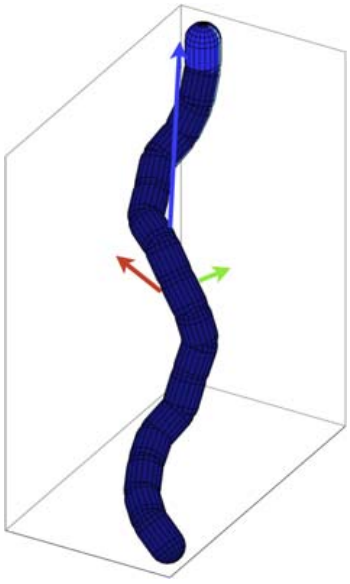

Figure 7. An example of the approximate axes of the virtual chassis for a position in the pipe crawling gait.

of all the links in robot to some centerline. If we define this centerline as the set of points, $l(s) = \mathbf{a} + \mathbf{vs}$, the distance d_i of a point $\mathbf{p_i}$ to this line is

$$d_i = |(a + ((\mathbf{p_i} - \mathrm{a}) \cdot \mathrm{v})\mathrm{v} - \mathbf{p_i})| \tag{7}$$

The objective function for optimizing the centerline parameters **a** and **v** is the sum-squared error of the distance from each link to the centerline d_i compared to the mean distance of all the links to the centerline $\bar{d}$,

$$\text{error} = \sum_{i=1}^{n} (d_i - \bar{d})^2 \tag{8}$$

Because this objective function is nonconvex, random restarts in the vicinity of the initial SVD solution are used to ensure that the optimization does not converge to a local minimum that does not reflect the true centerline of the robot's shape.

For this gait, the z axis is chosen to align with the optimized centerline vector **v**. An arbitrary reference link (in our case, the middle link) is chosen to define the frame's rotation about the centerline. This is achieved by aligning the y axis with the vector that describes the line perpendicular to the centerline that passes through the reference link. Lastly, the desired x axis is calculated from the cross product of the z and y axes, to ensure a right-handed coordinate frame. A comparison of the motions of pipe crawling in an initial head-fixed body frame and the virtual chassis body frame is shown in Figure 8.

4.4. *Helix - Pole Climbing*

Pole climbing uses a different range of parametrizations of the helix gait which are more appropriate for climbing on the outsides of poles and pipe. The base shape of the robot is still a helix, but one in which the diameter is much wider

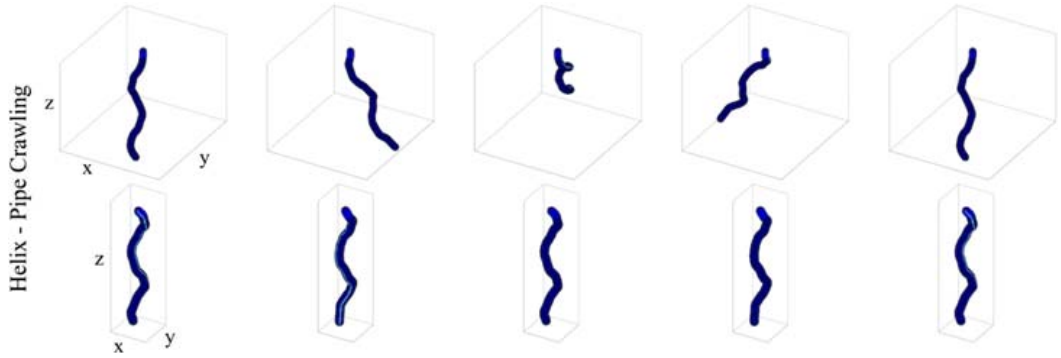

Figure 8. A montage of the robot in pipe crawling, comparing the motions in a body frame fixed to the head link (top row) and the virtual chassis body frame (bottom row).

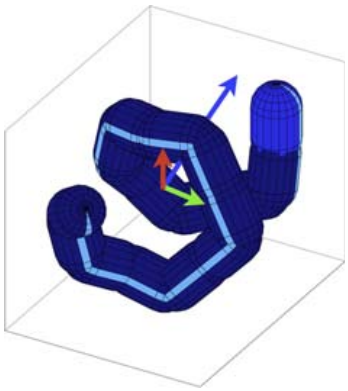

Figure 9. An example of the approximate axes of the virtual chassis for a position in the pole climbing gait.

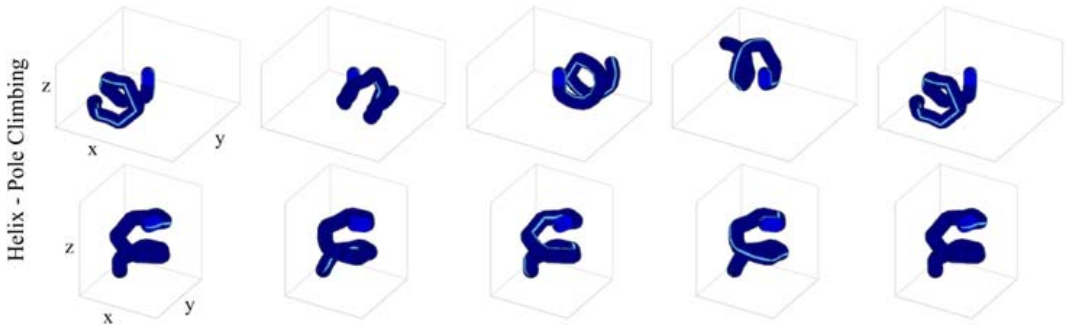

Figure 10. A montage of the robot in pole climbing, comparing the motions in a body frame fixed to the head link (top row) and the virtual chassis body frame (bottom row).

and the pitch is less steep (Figure 9). To achieve these qualities, we choose large values for amplitude A, and smaller values of spatial frequency Ω.

As in pipe crawling, the coordinate frame can again be optimized beyond what is provided by SVD. In fact, it becomes even more beneficial as the misalignment of the first principal moment of inertia with the true centerline of the robot's helix is much more pronounced. This effect is primarily attributable to the "longest" direction of the robot's shape becoming more ambiguous, as the increased diameter of the helix starts to approach the overall length of the helix. The virtual chassis body frame for pole climbing is calculated with the same secondary optimization as pipe crawling, and the result is shown in Figure 10.

4.5. Real-Time Implementation

Calculating the virtual chassis using the SVD procedure in Section 3 can easily be performed in real time. However, when using the refined virtual chassis body frame in pipes, the secondary optimization significantly slows the body frame

calculations. To address this limitation, we precompute lookup tables for the body frames, sorted by gait parameters. For pipe crawling and pole climbing, we require three lookup parameters from the gait equations (1) and (2): temporal position in the gait cycle ωt, amplitude A, and spatial frequency Ω. To perform the table lookup, we can fit gait parameters to the to feedback joint angles in real time using an extended Kalman filter (EKF), similar to the one presented in the following section.

5. Application – Orientation Estimation

In order to provide better feedback to an operator, we would like to fuse the readings from redundant sensors distributed throughout our robot into a unified estimate of its orientation. Each link of our lab's snake robot contains gyros and accelerometers for sensing the robot's motion in the world. A number of methods exists for fusing sensor data in robotic systems [21]. One of the most commonly used methods of fusing redundant and complimentary data is the EKF [34].

The true process model that describes the pose of our robot as it locomotes is complex, nonlinear, and largely unknown. However, in this section we will show that representing the robot's motion in the virtual chassis body frame mitigates these problems, to the point where a simple constant velocity process model can be used. This is due to the virtual chassis separating the robot's internal shape changes, which can be estimated accurately from the robot's joint angles, from its external motion, which is much simpler from the perspective of the robot's averaged overall shape.

Our experiments compare the performance of the EKF run in the virtual chassis vs. a fixed body frame for the snake robot executing the rolling gait, using motion capture data as ground truth. The rolling gait was chosen because it undergoes more rapid motion than other gaits, and because the gait's simpler shape allows for an easy comparison of the robot's estimated pose to the motion capture ground truth.

5.1. Process Model

The state of the robot consists of parameters that describe the robot's internal shape and orientation. The state representation for the shape of the robot uses the rolling gait's two parameters and their respective first derivatives. Combining these with four variables for representing the robot's quaternion orientation, and three variables for representing the body frame angular velocity, results in the 11-dimensional state vector,

$$X = [A \quad \dot{A} \quad \xi \quad \dot{\xi} \quad q^T \quad \omega^T] \tag{9}$$

where A and ξ are the gait parameters from (1), $\mathbf{q} = [q_1\ q_2\ q_3\ q_4]^T$ is the orientation quaternion vector in the world frame and $\omega = [\omega_x \quad \omega_y \quad \omega_z]^T$ are the robot's angular velocities in the body frame.

The gait parameters at each timestep are updated by the estimate of their first derivatives, and the first derivatives are assumed to be constant across timesteps,

$$\hat{A}_t = A_{t-1} + \dot{A}_{t-1} \cdot dt \tag{10}$$

$$\hat{\xi}_t = \xi_{t-1} + \dot{\xi}_{t-1} \cdot dt. \tag{11}$$

The quaternion orientation of the robot is updated by the angular velocities and the update timestep, according to the discrete time update equations,

$$\hat{q}_t = \exp(-\frac{1}{2}\mathbf{\Psi} \cdot dt)\mathbf{q_{t-1}} \tag{12}$$

$$\mathbf{\Psi} = \begin{bmatrix} 0 & \omega_x & \omega_y & \omega_z \\ -\omega_x & 0 & -\omega_z & \omega_y \\ -\omega_y & \omega_z & 0 & -\omega_x \\ -\omega_z & -\omega_y & \omega_x & 0 \end{bmatrix} \tag{13}$$

A closed-form solution for this update is presented by van der Merwe et al. [35], which guarantees that the resulting quaternion is of unit norm. As with the derivatives of the gait parameters, the body frame angular velocities of the robot $\boldsymbol{\omega}$ are assumed to be constant across timesteps.

The simplicity of this constant velocity model would seemingly cause problems, given the complex motions of a snake robot. However, this illustrates a key benefit of using the virtual chassis body frame. Figure 11 shows state estimates of the body frame angular velocity for the same rolling trial in both the virtual chassis and fixed body frames. Both plots show the same motion, where the robot is sitting still, quickly starts rolling, and then stops. Note that in the virtual chassis body frame, the angular velocities are essentially zero throughout the run, even during the abrupt start and stop of the robot's motion.

The practical advantage of being able to use such a generic model is in its applicability to any motion of the snake robot. Despite the relatively intuitive motion of the rolling gait, in virtually all of the other gaits that our lab has developed [3], the motion of the robot is significantly more complex, and any process model that predicts an individual link's orientation would depend on both the specific gait and the robot's (mostly unknown) interaction with the world. The virtual chassis greatly reduces the nonlinear effects of gait motion and world interaction, allowing the generic model described here to be applicable to a wide range of gaits and environments.

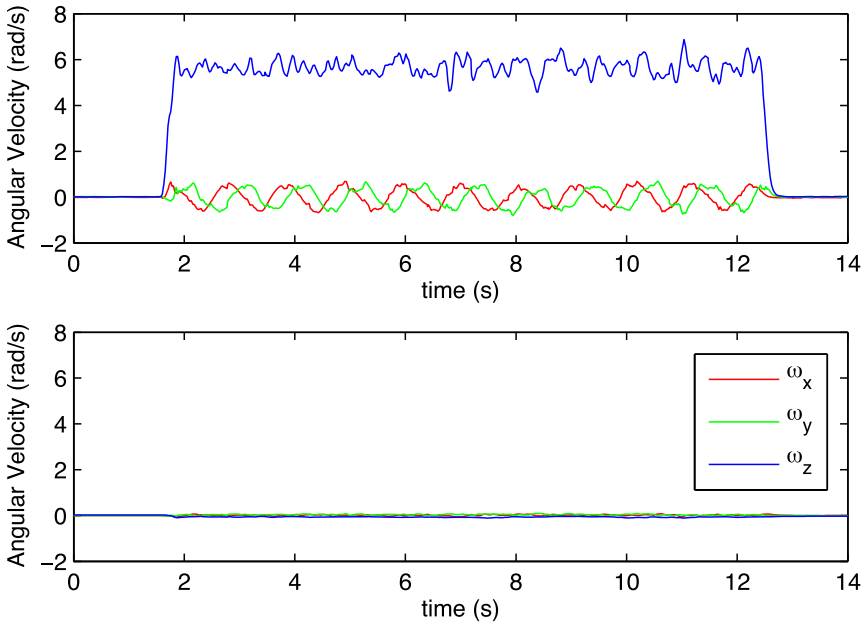

Figure 11. A comparison of estimated angular velocities for the same motion, observed in a body frame fixed to the middle link (upper plot) and a body frame aligned with the virtual chassis (lower plot). The red, green, and blue lines are respectively the x, y, and z body frame angular velocities.

5.2. *Measurement Model*

The snake robot provides feedback measurements from single-axis joint angle encoders, 3-axis accelerometers, and 2-axis gyros located in each link. The accelerometers measure the combined effects of gravity and the accelerations of each link in the world. The gyros directly measure the angular velocity of each link in the world. The measurement model generates expected readings for all of these sensors, given the robot's current state estimate. This means that the EKF measurement vector has dimensions, where n is the total number of links in the robot.

$$\mathbf{z} = [\quad \boldsymbol{\theta}^T \quad \boldsymbol{\alpha}^T \quad \boldsymbol{\gamma}^T \quad]. \tag{14}$$

In (14), each element is a vector containing the measurements of a corresponding sensor type for all the links throughout the robot. $\boldsymbol{\theta}$ is the vector of joint angles for each link, $\boldsymbol{\alpha}$ is the vector of accelerometer readings for each link, and $\boldsymbol{\gamma}$ is the vector of gyroscope measurements for each link.

Joint angles are predicted from the gait equation (1) using the current estimated gait parameters,

$$\hat{\theta} = [\bar{\theta}_1 \ldots \bar{\theta}_n]^T. \tag{15}$$

Predicted accelerometer and gyro readings are generated by numerically differentiating the position and orientation of the robot at different timesteps. The pose of each link can be constructed from the forward kinematics of the joint angles predicted in (15). Using the estimated derivatives of the gait parameters, $\dot{A}$ and $\dot{\xi}$, joint angles at nearby timesteps can be generated from which the corresponding shapes can be constructed.

Predicted accelerometer measurements for each link in the robot are generated by combining the gravity offset (determined from the robot's estimated orientation) with the internal accelerations due to that link's motion in the body frame

$$\hat{\boldsymbol{\alpha}}^i = \hat{\boldsymbol{\alpha}}^i_{\text{gravity}} + \hat{\boldsymbol{\alpha}}^i_{\text{motion}}. \tag{16}$$

Acceleration due to motion of the robot is predicted by double differentiating the estimated positions of the links with respect to time. Due to the simplified process model, the body frame acceleration of the robot in the world is assumed to be zero. Acceleration due to gravity is predicted by transforming the estimated gravity vector $\mathbf{g}$ into the frame of each link

$$\hat{\boldsymbol{\alpha}}^i_{\text{gravity}} = \mathbf{M}^i\mathbf{R}\mathbf{g} \tag{17}$$

where $\mathbf{M}^i$ is the rotation matrix that describes the orientation of link i in the body frame and $\mathbf{R}$ is the rotation matrix representation of the quaternion pose $\mathbf{q}$ in the state vector (9). For our work, $\mathbf{g}$ is assumed to be oriented along the z-axis of the world frame, where g is gravitational acceleration,

$$\mathbf{g} = [0 \quad 0 \quad g]^T. \tag{18}$$

The predicted gyro measurements for each link are similarly generated by differentiating link orientations at two nearby timesteps. If $\mathbf{M}_{\text{i,t}}$ and $\mathbf{M}_{i,t-1}$ are rotation matrices that describe the orientations of link i in the body frame at two timesteps, then gyro measurements due to the internal motion of the gait at two timesteps, t and $t-1$ can be approximated by

$$\begin{bmatrix} 1 & -\bar{\omega}^i_z & -\bar{\omega}^i_y \\ -\bar{\omega}^i_z & 1 & \bar{\omega}^i_x \\ -\bar{\omega}^i_y & \bar{\omega}^i_x & 1 \end{bmatrix} = \frac{\mathbf{M}^i_{\text{t}}(\mathbf{M}^i_{\text{t-1}})^{-1}}{dt}. \tag{19}$$

The predicted gyro measurements for each link taking into account the angular velocities of the entire robot are simply the angular velocities from (19) plus the angular velocities of the robot from the current state estimate, (9), transformed into the coordinate frame of each link using $\mathbf{M}_{\text{i,t}}$

$$\hat{\boldsymbol{\gamma}}^i_{\text{t}} = \bar{\boldsymbol{\omega}}^i + (\mathbf{M}^i_{\text{t}})^{-1}\hat{\boldsymbol{\omega}}_{\text{t}}. \tag{20}$$

The measurement model for the prediction of inertial data is where the choice of body frame comes into play. The robot's estimated body frame angular velocity affects both the predicted accelerometer and gyro measurements. The process model's assumptions of constant angular velocity between timesteps are much more accurate in the virtual chassis, where the body frame stays relatively stable throughout its motion, compared to a fixed body frame that tumbles in the world frame as the robot moves.

5.3. *Experiment*

To measure the accuracy of estimating the robot's pose from inertial sensors, we gathered ground-truth data of the robot's orientation using a motion capture system. Each experiment consisted of executing the rolling gait with fixed commanded parameters on a flat concrete floor. The motion capture system recorded the 3D position of IR reflective markers on three of the robot's links (head, middle, and tail), whereas the inertial and joint angle data used for the state estimation were logged from the robot's sensors.

To compute the roll, pitch, and yaw of the robot in each frame, the motion capture point cloud data were spatially clustered into groups for each of the marked links. The geometric center of mass of each point cloud was used as an approximation for each link centers $\mathbf{p}_{\text{head}}$, $\mathbf{p}_{\text{mid}}$, and $\mathbf{p}_{\text{tail}}$.

To compare the estimated orientation from the EKF to measured orientation motion capture, a ground-truth body frame was set such that the x axis was collinear with the vector from the center of the tail to the center of the head link and the y axis was on the line perpendicular to the tail-head line and passing through center of the middle link (Figure 12)

$$\mathbf{x} = \mathbf{p}_{\text{head}} - \mathbf{p}_{\text{tail}} \tag{21}$$

$$\mathbf{y} = \mathbf{P}_{\text{tail}} + ((\mathbf{P}_{\text{mid}} - \mathbf{P}_{\text{tail}}) \cdot \mathbf{x})\mathbf{x} - \mathbf{P}_{\text{mid}}. \tag{22}$$

The z axis, $\mathbf{z}$, is calculated from the cross product of $\mathbf{x}$ and $\mathbf{y}$, and the lengths of these orthonormal vectors are normalized to form a right-handed frame expressed as the rotation matrix

$$\mathbf{R} = \left[\frac{\mathbf{x}}{|\mathbf{x}|} \quad \frac{\mathbf{y}}{|\mathbf{y}|} \quad \frac{\mathbf{z}}{|\mathbf{z}|}\right]. \tag{23}$$

This rotation matrix is calculated in a similar manner for the robot's estimated shape as well. In order to better interpret the robot's motion, both the estimated and ground-truth rotation matrices were converted into Euler angles in the X-Y-Z intrinsic convention. This convention is the classical roll–pitch–yaw that is commonly used to describe the attitude of aircraft.

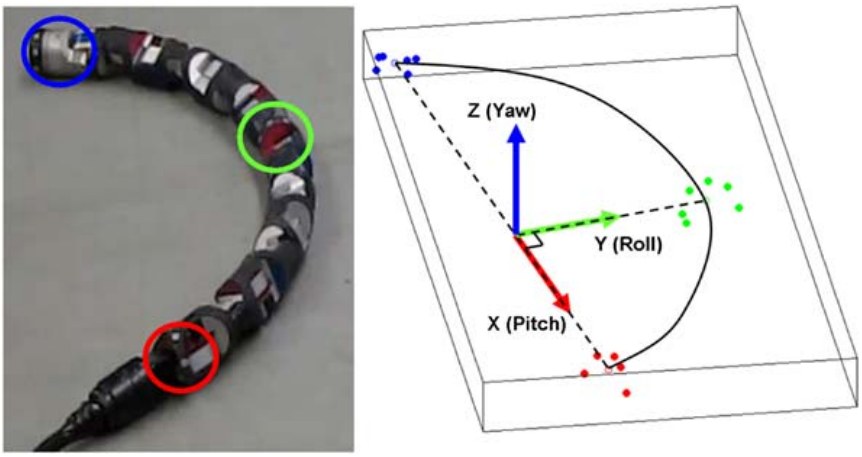

Figure 12. Images showing the snake robot with reflective IR markers and ground-truth frame assignment from motion capture point clouds.

The 3D trajectories of the link centers of mass were zero-lag low passed to remove noise from IR markers rolling in and out of view of the motion capture cameras. For each of the experimental runs, the robot was driven a distance, paused, and returned to its approximate starting position (Figure 13). Error for each of roll, pitch, and yaw was calculated by taking the absolute value of the difference between the estimated body frame orientations and the ground-truth orientations of the fitted frame.

We ran a total of 11 trials of in which we executed the rolling gait at different speeds: Slow Speed: 2 trials at 0.2 gait cycles/s, Medium Speed: 5 trials at 0.5 cycles/s, and Fast Speed: 4 trials at 1.0 cycles/s.

5.4. Results

Figure 14 shows a representative pitch error vs. time for one of the experimental trials. In order to highlight the differences in performance of the three approaches for estimating the robot's orientation, we only considered times when the robot was moving. For the 11 trials, we computed and compared the average orientation error across different gait speeds and estimator types, as shown in Figures 15–17.

Estimated orientation errors of the EKF were compared using both the virtual chassis and fixed body frames at each of these speeds. Use of the virtual chassis significantly reduced error of the estimated pitch of the robot, with the improvement being more apparent at higher speeds of rolling. To provide a fair comparison of filtering in the different body frames, the process and measurement noise parameters for the fixed frame and virtual chassis were tuned separately for best performance. Overall, the EKF running in a fixed frame required significantly higher levels of process noise to prevent filter divergence, while the EKF using the virtual chassis was much less sensitive to tuning parameters.

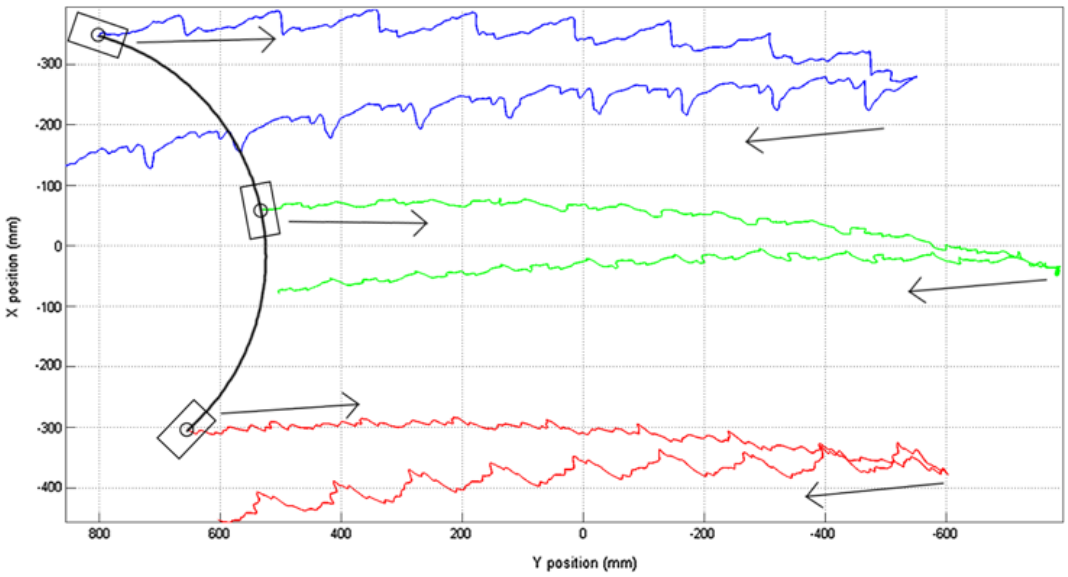

Figure 13. A representative trajectory of a motion capture trial. The robot is represented by the black arc. The trajectories of each of the sets of marks are shown by the colored traces, moving from left to right, then returning to the left.

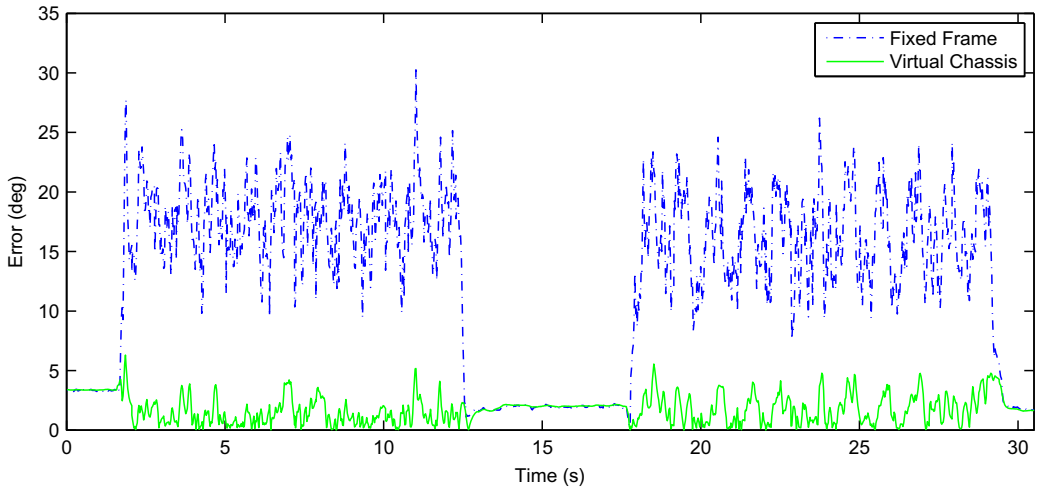

Figure 14. Absolute value of pitch error vs. time for the fixed frame and virtual chassis estimator in a fast speed trial.

The virtual chassis did not improve the snake robot's average estimated yaw at any of the different speeds that were tested. Additionally, the average and standard deviations of the errors of the yaw estimates were an order of magnitude above the errors of estimated pitch and roll. This is to be expected, as the robot's gyros and accelerometers can only provide absolute orientation with respect to gravity. Thus, the yaw orientation estimates are essentially an integration of estimated yaw velocities over the course of each trial that show significant drift due to integration error.

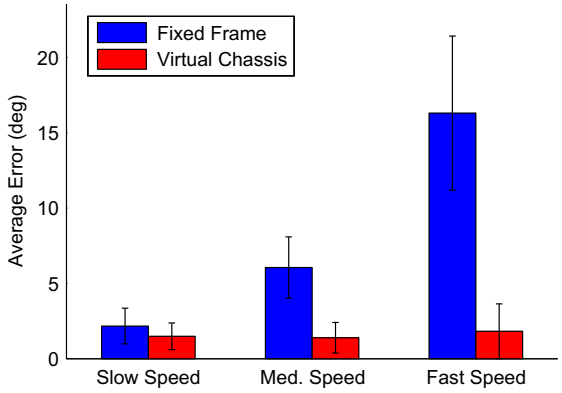

Figure 15. Averaged absolute value of error in estimated pitch comparing different state representations, grouped by speed of the trials.

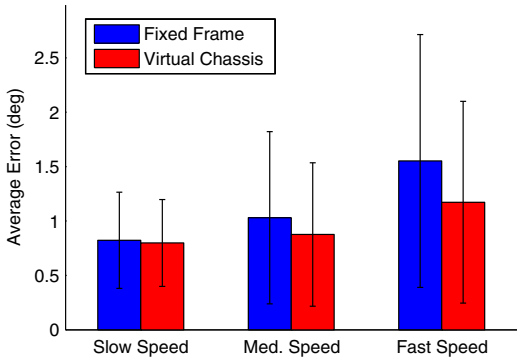

Figure 16. Averaged absolute value of error in estimated roll comparing different state representations, grouped by speed of the trials.

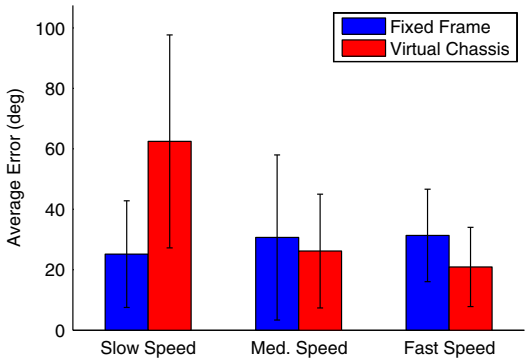

Figure 17. Averaged absolute value of error in estimated yaw comparing different state representations, grouped by speed of the trials.

6. Conclusions

The virtual chassis is a framework that represents a snake robot's pose in a simplified and intuitive manner. By leveraging the symmetry of the robot's shape as

it executes gaits, we have introduced a body frame that separates the internal motion due to the shape changes of a gait from the external motion caused by a gait's interaction with the world. This representation is aligned with the natural notions of position and orientation of the snake robot that previously rested only with a human operator. Again, we should note that the virtual chassis can be applied to any shape that has distinct principal components, not only the gaits presented in their paper. This includes noncyclic motions and transitional motions between different gaits.

The advantages of the virtual chassis body frame allow us to treat articulated mobile robots more like wheeled robots, where internal shape changes smoothly propel the robot through the world. In particular, we can now use simple models to accurately approximate what has traditionally been considered complex motion. We demonstrated the practical advantages of this by using an EKF with a simple process model to accurately estimate our snake robot's orientation while undergoing highly dynamic motions. While results were presented for the rolling gait, our group has successfully used this same framework to estimate the robot's orientation in a wide range of motions and environments.

Acknowledgments

The authors would like to acknowledge the help provided by the members of the Biorobotics Lab and the Robotics Institute. In particular, we would like to thank Ross Hatton, Matt Tesch, Glenn Wagner, Justin MacEy, Mike Schwerin, and Ben Brown.

This work was accomplished with the assistance of the DARPA M3 program, contract number W911NF1110061.

References

1. G. Chirikjian and J. Burdick, The kinematics of hyper-redundant robot locomotion, *IEEE Trans. Robot. Automat.*, **11**(6), 781–793 (1995).
2. C. Wright, A. Buchan, B. Brown, J. Geist, M. Schwerin, D. Rollinson, M. Tesch and H. Choset, Design and architecture of the unified modular snake robot, *IEEE Int. Conf. Robot. Automat. (ICRA 2012)*, Minneapolis, MN (in press).
3. M. Tesch, K. Lipkin, I. Brown, R. L. Hatton, A. Peck, J. Rembisz and H. Choset, Parameterized and scripted gaits for modular snake robots, *Adv. Robot.*, **23**, 1131–1158 (2009).
4. A. A. Transeth, *Modelling and Control of Snake Robots*, Ph.D. dissertation, Norwegian University of Science and Technology (NTNU) (2007).
5. B. Jayne, Kinematics of terrestrial snake locomotion, *Copeia*, 915–927 (1986).
6. J. Gray, The mechanism of locomotion in snakes, *J. Exp. Biol.* **23**(2), 101–123 (1946).
7. S. Hirose, *Biologically Inspired Robots*. Oxford University Press, New York, NY (1993).
8. B. Jones and I. Walker, Kinematics for multisection continuum robots, *IEEE Trans. Robot.*, **22** (1), 43–55, (2006).

9. S. Ma, Analysis of creeping locomotion of a snake-like robot, *Adv. Robot.* **15**(2), 205–224 (2001).
10. J. Burdick, J. Radford and G. Chirikjian, A sidewinding locomotion gait for hyper-redundant robots, *Adv. Robot.* **9**(3), 195–216 (1995).
11. D. Reznik and V. Lumelsky, Sensor-based motion planning in three dimensions for a highly-redundant snake robot, *Adv. Robot.* **9**(3), 255–280 (1995).
12. S. Yu, S. Ma, B. Li and Y. Wang, An amphibious snake-like robot with terrestrial and aquatic gaits, in: *IEEE International Conference on Robotics and Automation*, Shanghai, China, pp. 2960–2961 (2011).
13. OC Robotics – http://www.ocrobotics.com/ (2012).
14. Medrobotics Corporation – http://cardiorobotics.com/ (2012).
15. D. I. Goldman and D. L. Hu, The mechanics of slithering locomotion depend on the surroundings, *Am. Scientist*, **98**, 314–323 (2010).
16. A. Transeth, R. Leine, C. Glocker and K. Pettersen, 3-D snake robot motion: nonsmooth modeling, simulations, and experiments, *IEEE Trans. Robot.*, **24**, 361–376 (2008).
17. A. A. Transeth, R. I. Leine, C. Glocker, K. Y. Pettersen and P. l. LiljebAck, Snake robot obstacle-aided locomotion: modeling, simulations, and experiments, *IEEE Trans. Robot.*, **24**, 88–104 (2008).
18. A. Shapere and F. Wilczek, Geometry of self-propulsion at low Reynolds number, *J. Fluid Mech*., **198**, 557–585 (1989).
19. S. Kajita, F. Kanehiro, K. Kaneko, K. Fujiwara, K. Harada, K. Yokoi and H. Hirukawa, Resolved momentum control: humanoid motion planning based on the linear and angular momentum, in: *Proc. IEEE/RSJ International Conference on Intelligent Robots and Systems, 2003.(IROS 2003)*, Las Vegas, NV, Vol. 2, pp. 1644–1650 (2003).
20. R.L. Hatton and H. Choset, Geometric motion planning: the local connection, Stokes's theorem, and the importance of coordinate choice, *The Int. J. Robot. Res.* **30**(8), 988–1014 (2011).
21. R. Luo, C. Yih and K. Su, Multisensor fusion and integration: approaches, applications, and future research directions, *Sensors J., IEEE* **2**(2), 107–119 (2002).
22. W. Park, Y. Liu, Y. Zhou, M. Moses and G.S. Chirikjian, Kinematic state estimation and motion planning for stochastic nonholonomic systems using the exponential map, *Robotica* **26**, 419–434 (2008).
23. E. Lefferts, F. Markley and M. Shuster, Kalman filtering for spacecraft attitude estimation, *J. Guidance* **5**, 417–429 (1982).
24. I. Bar-Itzhack and Y. Oshman, Attitude determination from vector observations quaternion estimation, *IEEE Trans. Aerospace Electronic Syst.* **21**(1), 128–136 (1985).
25. C. Wright, A. Johnson, A. Peck, Z. McCord, A. Naaktgeboren, P. Gianfortoni, M. Gonzalez-Rivero, R. L. Hatton and H. Choset, Design of a modular snake robot, in: *Proc. IEEE International Conference on Intelligent Robots and Systems*, San Diego, CA, October (2007).
26. H. Ohno and S. Hirose, Design of slim slime robot and its gait of locomotion, in: *Proc. 2001 IEEE/RSJ International Conference on Intelligent Robots and Systems*, Maui, HI, pp. 707–715 (2001).
27. R. M. Murray, Z. Li and S. S. Sastry, *A Mathematical Introduction to Robotic Manipulation,* CRC Press, Boca Raton, FL (1994).
28. L.N. Trefethen and D. Bau, *Numerical Linear Algebra*. SIAM, Philadelphia, PA (1997).
29. E. Ziegel, W. Press, B. Flannery, S. Teukolsky and W. Vetterling, *Numerical Recipes: The Art of Scientific Computing,* **29**(4) (1987).

30. R. Bro, E. Acar and T. Kolda, Resolving the sign ambiguity in the singular value decomposition, *J. Chemometr.* **22**(2), 135–140 (2008).
31. W. Mosauer, A note on the sidewinding locomotion of snakes, *The Am. Naturalist* **64**(691), 179–183 (1930).
32. J. Burdick, J. Radford and G. Chirikjian, A sidewinding locomotion gait for hyper-redundant robots, *Robot. Automat.* **3**, 101–106 (1993).
33. A. Nelder and R. Mead, A simplex method for function minimization, *Comput. J.* **7**, 308–313 (1965).
34. H. Choset, K.M. Lynch, S. Hutchinson, G. Kantor, W. Burgard, L.E. Kavraki and S. Thrun, *Principles of Robot Motion: Theory Algorithms, and Implementations*. MIT Press, Boston, MA (2005).
35. R. Van Der Merwe, E. Wan, and S. Julier, Sigma-point kalman filters for nonlinear estimation and sensor-fusion, in: *Proc. AIAA Guidance, Navigation & Control Conference*, Citeseer, pp. 5120–5159 (2004)

About the Authors

Austin Buchan received his BS in electrical and computer engineering from Carnegie Mellon University in May 2010. He is currently pursuing a PhD at the University of California Berkeley under Ronald Fearing in the Biomimetic Millisystems Laboratory. His research interests include biologically inspired sensing for mobile autonomous systems and sensor fusion techniques for compute constrained applications.

Howie Choset is a professor of robotics at Carnegie Mellon University, where he conducts research in path planning, motion planning, estimation, mechanism design, and hybrid controls. Much of this work has two foci: snake robots for search and rescue, manufacturing and medical robotics, and coverage for de-mining and autobody painting. He directs the undergraduate robotics minor at Carnegie Mellon University and teaches an overview course on robotics which uses series of custom developed Lego Labs to complement the course work. His students have won Best Paper awards at the RIA in 1999 and ICRA in 2003, he has been nominated for Best Papers at ICRA in 1997 and IROS in 2003, 2007, and 2011, and won Best Paper at IEEE Bio Rob in 2006. In 2002, the MIT Technology Review elected him as one of its top 100 innovators in the world under 35. In 2005, MIT Press published a textbook, lead authored by him, entitled principles of robot motion.

Dave Rollinson received a BS in mechanical engineering in 2006 and MS in robotics in 2010, both from Carnegie Mellon University, and he currently is a PhD student in the Robotics Institute at Carnegie Mellon. From 2006 to 2009, he worked as a mechanical engineer for RedZone Robotics, making systems to inspect large diameter sewers in the USA, Canada, and Singapore. His research focuses on finding intuitive ways to analyze and control snake robots.